Int. J. Heat Mass Transfer. Vol. 35, No. 10, pp. 2515–2526, 1992
Printed in Great Britain

0017–9310/92 $5.00 + 0.00

A numerical study of heat transfer due to an axisymmetric laminar impinging jet of supercritical carbon dioxide

JOO-KYUN KIM and TOSHIO AIHARA
Institute of Fluid Science, Tohoku University, 2-1-1 Katahira, Aoba-ku, Sendal 980, Japan

(*Received* 9 *July* 1990 *and in final form* 12 *June* 1991)

Abstract—The physical properties of a supercritical fluid vary markedly as the temperature and the pressure approach its critical point. In this paper, heat transfer due to an axisymmetric laminar impinging jet onto a flat wall surface of uniform temperature is analyzed numerically, taking into account the temperature- and pressure-dependence of all physical properties of supercritical carbon dioxide. Numerical solutions are obtained for the jet Reynolds numbers 500–2000, the jet pressures 7.4–8.4 MPa, the jet mouth-to-surface distances 1–4 times the jet nozzle diameter, and the temperature difference between the jet mouth and flat wall from 10 to 150 K. The differences between the supercritical pressure and the atmospheric pressure for the flow field and the temperature field are investigated. Also, the effects of the pressure and the temperature of the jet, the jet mouth-to-surface temperature difference and the jet Reynolds number on the heat transfer characteristic are examined. A correlating equation of estimating the value of the local Nusselt number for the supercritical carbon dioxide from the constant-property solution is proposed and the agreement between the present correlation and numerical results is within 10%.

1. INTRODUCTION

THE HEAT transfer of the impinging jet has been of interest to engineers for many years because of its wide applications. A turbulent jet impinging on a solid body can easily attain high heat transfer characteristics by virtue of vortex motions and intensive large-scale eddies [1–3]. However, a laminar impinging jet is also encountered in practice, especially in the case where the jet mouth-to-surface distance is short and a high stagnation pressure is not desirable. Many experimental and theoretical investigations have been carried out on the heat and mass transfer of a laminar impinging jet [4–8]. Recently, the present authors [9] studied numerically the effects of the temperature-dependent fluid properties on the heat transfer due to an axisymmetric impinging gas jet onto a flat solid surface of a uniform temperature, with the large temperature difference between the jet and the solid surface at a pressure of 0.1 MPa.

The necessity of the heat transfer data of supercritical fluids is increasing in various industrial applications. In the supercritical region, a small variation in the temperature and pressure of the fluid produces great changes in its thermophysical properties, and the heat transfer characteristic is strongly influenced by the temperature- and pressure-dependence of physical properties. Existing research on the forced convective heat transfer of supercritical fluids is mainly carried out for a straight circular tube [10–12]. To the authors' knowledge, there is no reference on heat transfer due to an impinging jet of supercritical fluid, except for the authors' report in the near-critical region of carbon dioxide [13].

In the present study of the heat transfer due to an axisymmetric laminar jet impinging normal to a flat solid surface of uniform temperature, the attention is focused on the supercritical region of carbon dioxide where the physical properties have strong pressure and temperature dependences. The numerical analysis is carried out by a control volume method, taking into account the pressure and temperature dependence of all physical properties. The differences between the supercritical pressure and the atmospheric pressure for the flow field and the temperature field are discussed, and the effects of the pressure- and temperature-dependence of fluid properties on heat transfer characteristics are investigated for various conditions. To attain the estimating equation for the local Nusselt number of the supercritical carbon dioxide from the present numerical solutions, the reference temperature method and the property correction method are examined, and consequently a correlating equation for the supercritical carbon dioxide is proposed.

2. MATHEMATICAL FORMULATION AND NUMERICAL PROCEDURE

2.1. *Mathematical formulation*

The flow geometry and solution domain to be considered are shown in Fig. 1. A laminar jet issues from a circular tube of diameter d at an average velocity $\bar{u}$, and impinges perpendicularly onto a flat solid surface at a distance l from the jet mouth.

For simplification, some assumptions are introduced as follows:

NOMENCLATURE

c_f	local friction coefficient, equation (7)
c_p	specific heat of fluid at constant pressure
d	diameter of nozzle
D	diffusivity of fluid
h_d	local mass transfer coefficient
h_x	local heat transfer coefficient, equation (8)
i	specific enthalpy
I	dimensionless specific enthalpy, Table 1
l	distance between jet mouth and solid surface
L	dimensionless distance between jet mouth and solid surface, Table 1
Nu	local Nusselt number
$(Nu)_r$	local Nusselt number modified by the fluid property at the reference temperature
p	pressure
P	dimensionless pressure, Table 1
p_c	critical pressure of fluid
Pe	Peclet number, $Pr\,Re$
Pr	Prandtl number, $\mu_j c_{pj}/\lambda_j$
Re	jet Reynolds number, $\rho_j \bar{u} d/\mu_j$
S	source term in equation (4)
Sc	Schmidt number, $\mu/(\rho D)$
Sh	local Sherwood number, $h_d d/D$
St	local Stanton number, $Nu/(Re\,Pr)$
T	temperature
T_c	critical temperature of fluid
T_{pc}	pseudocritical temperature of fluid
u, v	velocity components in axial- and radial-directions
U, V	dimensionless velocity components in axial- and radial-directions, Table 1
$\bar{u}$	average velocity at jet mouth
u_0	jet velocity at the center of nozzle exit
x, r	axial and radial coordinates, Fig. 1
X, R	dimensionless axial and radial coordinates, Table 1.

Greek symbols

Γ	coefficient of diffusion term, Table 2
θ	dimensionless temperature, Table 1
λ	thermal conductivity of fluid
μ	absolute viscosity of fluid
ρ	density of fluid
τ_w	wall shear stress, $\mu_w(\partial V/\partial X)_w$
ϕ	dimensionless variable, equation (4)
ψ	dimensionless stream function, $\int UR\,dR$.

Subscripts

j	value at jet mouth
w	value at wall surface
0	value at stagnation-point, unless specified.

Superscript

*	value normalized by fluid properties at jet temperature.

(1) The flow is steady, axisymmetric, and laminar.

(2) The size of the solid surface is sufficiently large and the wall thickness of the jet nozzle is negligible in comparison with the jet diameter.

(3) The effects of gravity, viscous dissipation and radiation are neglected.

Hence, the governing equations are expressed as follows:

Mass conservation:

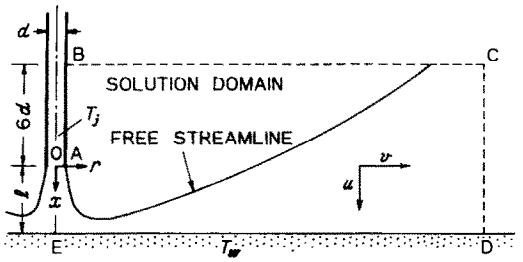

FIG. 1. Physical model and coordinate system.

$$\frac{\partial}{\partial x}(\rho u)+\frac{1}{r}\frac{\partial}{\partial r}(\rho r v)=0. \quad (1)$$

Axial momentum conservation:

$$\rho u\frac{\partial u}{\partial x}+\rho v\frac{\partial u}{\partial r}=-\frac{\partial p}{\partial x}+\frac{\partial}{\partial x}\left(2\mu\frac{\partial u}{\partial x}\right)+\frac{1}{r}\frac{\partial}{\partial r}\left\{r\mu\left(\frac{\partial u}{\partial r}+\frac{\partial v}{\partial x}\right)\right\}. \quad (2)$$

Radial momentum conservation:

$$\rho u\frac{\partial v}{\partial x}+\rho v\frac{\partial v}{\partial r}=-\frac{\partial p}{\partial r}+\frac{\partial}{\partial x}\left\{\mu\left(\frac{\partial v}{\partial x}+\frac{\partial u}{\partial r}\right)\right\}+\frac{1}{r}\frac{\partial}{\partial r}\left(2r\mu\frac{\partial v}{\partial r}\right)-\frac{2\mu v}{r^2}. \quad (3)$$

Energy conservation:

$$\rho u\frac{\partial i}{\partial x}+\rho v\frac{\partial i}{\partial r}=\frac{\partial}{\partial x}\left(\frac{\lambda}{c_p}\frac{\partial i}{\partial x}\right)+\frac{1}{r}\frac{\partial}{\partial r}\left(\frac{\lambda}{c_p}r\frac{\partial i}{\partial r}\right). \quad (4)$$

Applying the dimensionless variables listed in

Table 1. Dimensionless variables

X	R	L	U	V	P	I	θ	ρ^*	λ^*	μ^*	c_p^*
x/d	r/d	l/d	u/u_0	v/u_0	$(p-p_j)/\rho_j u_0^2$	$(i-i_j)/c_{pj}T_j$	$(T-T_j)/(T_w-T_j)$	ρ/ρ_j	λ/λ_j	μ/μ_j	c_p/c_{pj}

Table 1, we can represent the non-dimensional conservation equations in a general form as

$$\frac{1}{R}\left\{\frac{\partial}{\partial X}\left(\rho^* RU\phi - R\Gamma\frac{\partial\phi}{\partial X}\right) + \frac{\partial}{\partial R}\left(\rho^* RV\phi - R\Gamma\frac{\partial\phi}{\partial R}\right)\right\} = S \quad (5)$$

where ϕ stands for the dimensionless variables U, V, and I. The expressions of Γ and S for each dependent variable are given in Table 2, and c_p^*, λ^*, ρ^*, and μ^* are the functions of fluid temperature and pressure.

The reasonable locations of the boundaries BC and CD in Fig. 1 were examined minutely in a preliminary numerical experiment described in the Appendix. On the basis of the result, the boundaries BC and CD were determined to be located $6d$ above the jet mouth and $20d$ from the jet axis.

The boundary conditions to be considered are as follows:

$$\left.\begin{aligned}
&U = 1-4R^2, \quad \text{and} \quad V = I = 0 \\
&\qquad \text{at jet mouth, OA} \\
&U = V = \partial I/\partial R = 0 \quad \text{at jet nozzle, AB} \\
&\partial U/\partial X = \partial V/\partial X = I = 0 \\
&\qquad \text{at upper boundary, BC} \\
&\partial(\rho^* U)/\partial R = \partial(\rho^* RV)/\partial R = \partial I/\partial R = 0 \\
&\qquad \text{at outer boundary, CD} \\
&U = V = 0, \quad \text{and} \quad I = I(T_w) \\
&\qquad \text{at solid surface, DE} \\
&\partial U/\partial R = V = \partial I/\partial R = 0 \\
&\qquad \text{at axis of symmetry, EO.}
\end{aligned}\right\} \quad (6)$$

The local friction coefficient c_f, local heat transfer coefficient h_x, and local Nusselt number Nu are defined respectively as

$$c_f = \tau_w/(\rho_j u_0^2/2) = -(1/Re)(\partial V/\partial X)_w \quad (7)$$

$$h_x = \lambda_w(\partial T/\partial x)_w/(T_w - T_j) \quad (8)$$

$$Nu = h_x d/\lambda_w = (\partial\theta/\partial X)_w, \quad (9)$$

where the dimensionless temperature θ is calculated reversely from the dimensionless specific enthalpy I obtained by the numerical calculation, using a program package for thermophysical properties, PROPATH [14].

When the fluid properties are evaluated at a reference temperature T_r, the local Nusselt number is modified as

$$(Nu)_r = h_x d/\lambda_w = (\partial\theta/\partial X)_w(\lambda_w^*/\lambda_r^*). \quad (10)$$

With regard to the reference temperature, the T_j and T_w are examined in the present study.

2.2. *Numerical procedure*

The discretization of equation (5) is performed by the control-volume method and the formulation of the convection and diffusion terms in equation (5) are calculated by using a power law scheme of Patankar [15]. In the numerical calculation of the flow field, the line-by-line iteration technique coupled with a tri-diagonal matrix algorithm by the Semi-Implicit Method for Pressure-Linked Equation, SIMPLE, is used. Under-relaxation factors are employed for all variables in order to prevent a divergence of numerical solutions at each iteration. In the numerical calculation of the specific enthalpy, the Gauss–Seidel point-by-point method is used.

A non-uniform, 51×41 staggered grid system is adopted. Since every variable has a relatively steep gradient near the solid surface, the finest grid size of $0.005d$ is selected there; the grid sizes are then monotonically increased with distances from the solid surface, jet mouth, and axis of symmetry, respectively, but no increasing ratio of the grid size ever exceeds 1.2. It has been confirmed that finer grid sizes produce no significant change in the numerical results of all variables at each node in the solution domain.

The convergence of numerical solutions for the flow field is decided on the basis of the residual-source

Table 2. Variables in general form for governing equations

ϕ	Γ	S
1	0	0
U	$\dfrac{\mu^*}{2Re}$	$-\dfrac{\partial P}{\partial X}+\dfrac{1}{2Re}\left\{\dfrac{\partial}{\partial X}\left(\mu^*\dfrac{\partial U}{\partial X}\right)+\dfrac{1}{R}\dfrac{\partial}{\partial R}\left(R\mu^*\dfrac{\partial V}{\partial R}\right)\right\}$
V	$\dfrac{\mu^*}{2Re}$	$-\dfrac{\partial P}{\partial R}+\dfrac{1}{2Re}\left\{\dfrac{\partial}{\partial X}\left(\mu^*\dfrac{\partial U}{\partial R}\right)+\dfrac{1}{R}\dfrac{\partial}{\partial R}\left(R\mu^*\dfrac{\partial V}{\partial R}\right)\right\}-\dfrac{\mu^* V}{Re\,R^2}$
I	$\dfrac{\lambda^*}{2Pe\,c_p^*}$	0

criterion [16]; namely, the convergence of U, V, and P is considered to have been attained when the sum of the absolute residual sources for each iteration of the respective variables is less than 0.005 of the dimensionless jet flow rate. With regard to the specific enthalpy field, the convergence is considered to have been attained when the absolute specific enthalpy difference in two consecutive iterations at every grid point is less than 0.0005. The validity of these convergence criteria was examined by a preliminary numerical experiment for various grid systems.

With regard to the physical properties of carbon dioxide, the required data are taken out from the PROPATH program package and fed to the source program, so as to shorten the CPU time. The fluid physical properties at each grid point are evaluated at the respective temperature and pressure obtained by each iteration. The CPU time on an NEC ACOS/2000 computer in Tohoku University is 600–1200 s for each run.

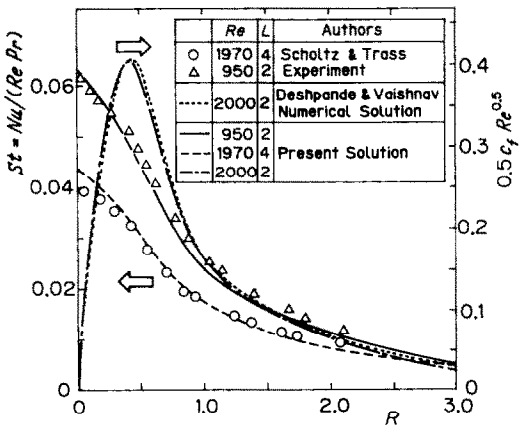

FIG. 2. Comparison of present constant property solutions with existing results by others.

3. NUMERICAL RESULTS AND DISCUSSION

3.1. *Constant property solutions (CPS)*

If one adopts a limit of $T_w/T_j \to 1$ in the present analysis, then the dimensionless properties, c_p^*, λ^*, ρ^*, and μ^* become unity, and the solution coincides with the constant-property solution. In Fig. 2, the present numerical solutions are compared with the existing experimental and theoretical results; the agreement is satisfactory [9]. The experimental data of Scholtz and Trass [4] were obtained by measuring the mass transfer rate from a naphthalene plate to an impinging round air jet with parabolic velocity profile at the jet mouth. The mass transfer data are converted to heat transfer data through the employment of a relation of heat mass transfer analogy, $Nu = (Pr/Sc)^{0.4}\, Sh$. The numerical solutions of Deshpande and Vaishnav [5] are those for the local friction coefficient on an impingement surface.

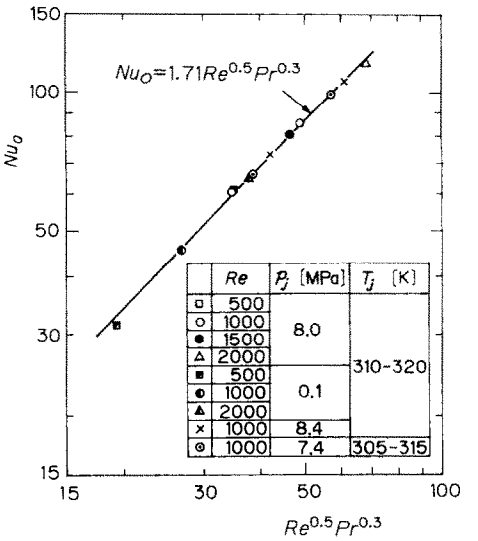

FIG. 3. Comparison in the stagnation-point Nusselt number between present constant property solutions and results of correlating equation (11).

Figure 3 shows a typical result in terms of the stagnation-point Nusselt number Nu_0 with constant-property solutions (CPS) for various Reynolds numbers Re, jet pressures p_j and jet temperatures T_j. The present CPS results for $500 \leqslant Re \leqslant 2000$, 0.1 MPa $\leqslant p_j \leqslant$ 8.4 MPa, and 305 K $\leqslant T_j \leqslant$ 320 K within an error of 3% can be well correlated with the following equation:

$$Nu_0^* = 1.71 Re^{0.5}\, Pr^{0.3}. \tag{11}$$

3.2. *Temperature- and pressure-dependence of physical properties*

The fluid physical properties vary markedly as the temperature and the pressure approach the critical point. According to the van der Waals equation which is stated for the thermodynamic behavior by the attractive and repulsive forces between molecules, the specific heat at constant pressure c_p of a fluid becomes infinity at the critical point [10]. The values of physical properties in the present study are evaluated by the data of the PROPATH program package, and the critical point of carbon dioxide is regarded as the critical pressure $p_c = 7.3825$ MPa and the critical temperature $T_c = 304.21$ K.

Figure 4 shows typical pressure- and temperature-dependences of specific heat c_p, thermal conductivity λ, density ρ, viscosity μ and Prandtl number Pr of carbon dioxide. In Fig. 4(a), the specific heat appears the maximum value near the critical point, and the temperature at which the specific heat reaches a peak is known as the pseudocritical temperature T_{pc}. As the pressure is increased, the temperature T_{pc} increases, but the maximum value of the specific heat decreases. For $1.0 \leqslant p/p_c \leqslant 1.15$, the pseudocritical temperature T_{pc} which is obtained from a relation of the pressure, the temperature and the specific heat by using the PROPATH can be introduced as

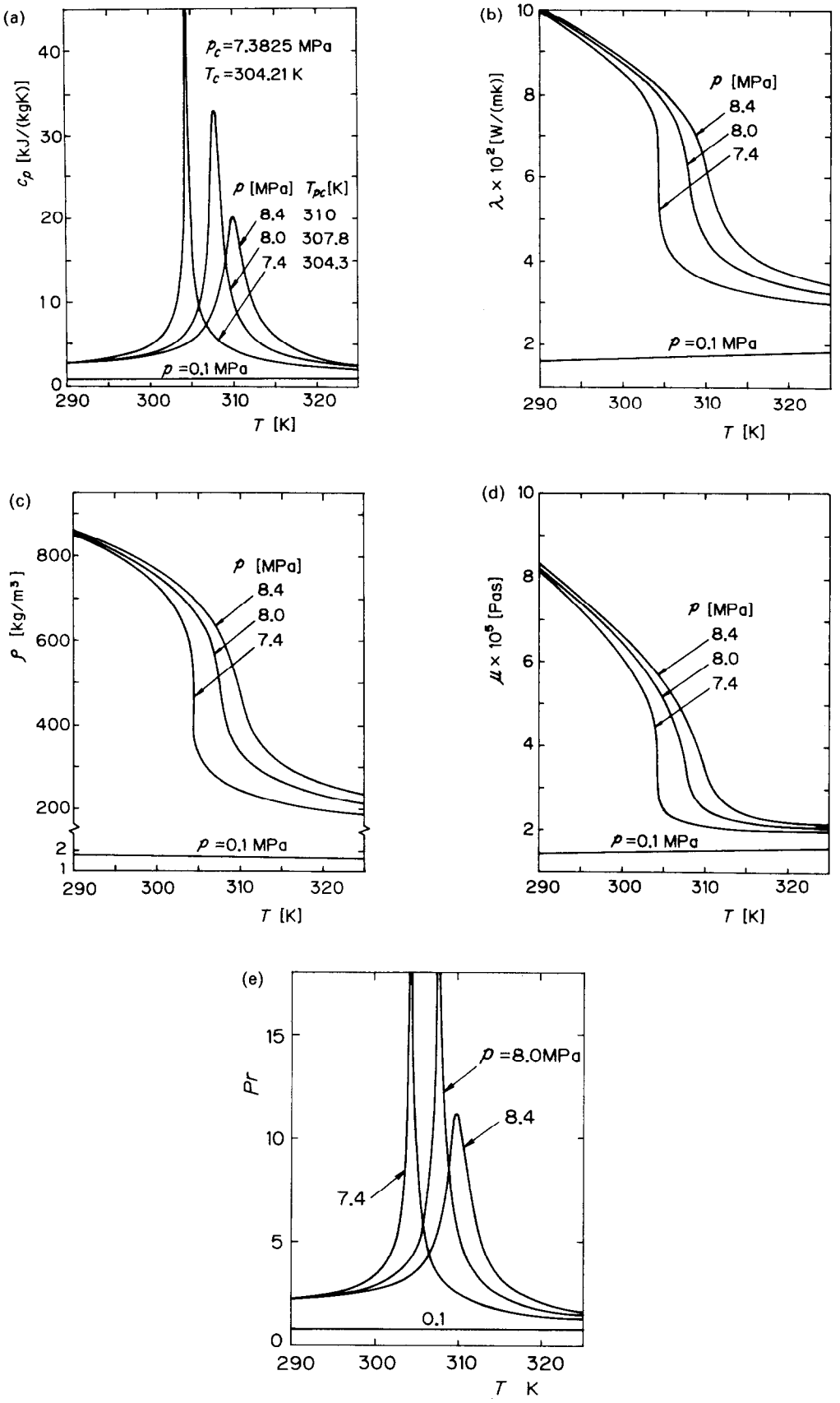

FIG. 4. Temperature- and pressure-dependence of carbon dioxide. (a) Specific heat; (b) thermal conductivity; (c) density; (d) viscosity; (e) Prandtl number.

$$T_{pc} = T_c(p/p_c)^{0.146}. \quad (12)$$

In Figs. 4(b)–(d), λ, ρ and μ show extreme temperature dependence in the vicinity of the T_{pc} corresponding to the pressure. Figure 4(e) shows a noticeable peak of Prandtl number by increasing the specific heat at the T_{pc} of each supercritical pressure.

Figure 5 shows a typical pressure- and temperature-dependence of the physical properties rendered by the properties at the temperature $T = 310$ K. The variation in the physical properties with the temperature at the supercritical pressure $p = 8.0$ MPa differs markedly from those at the atmospheric pressure $p = 0.1$ MPa. In the numerical calculations of variable property solution, all physical properties were employed the dimensionless value by each property at the jet temperature.

3.3. *Variable-property solution (VPS)*

The general effect of pressure- and temperature-dependent physical properties is to change the velocity and the temperature profile, yielding a different heat-transfer coefficient than would be obtained if properties were constant [17].

Figure 6 shows a typical distribution of streamlines and isotherms for $L = 2$, $Re = 1000$, $T_j = 310$ K and $T_w = 315$ K. In the figure, the jet mouth is located at a point of $X = 0$ and $R = 0$, and the right-half of the jet stream flows from the center ($R = 0$) to the right. Case (a) corresponds to the atmospheric pressure $p_j = 0.1$ MPa and case (b), to the supercritical pressure $p_j = 8.0$ MPa. In comparison of case (a) with case (b), the configuration of streamlines shows no substantial change except that the center of circulation in the case of $p_j = 8.0$ MPa is far from the jet mouth. However, the thickness of thermal boundary layer in the temperature field at $p_j = 8.0$ MPa becomes extremely thinner than that of $p_j = 0.1$ MPa. This seems to be influenced by the difference of pressure and temperature dependences of physical properties as shown in Figs. 4 and 5. Namely, it can be considered that temperature dependences of thermal conductivity and specific heat at the supercritical pressure affect remarkably on the temperature field.

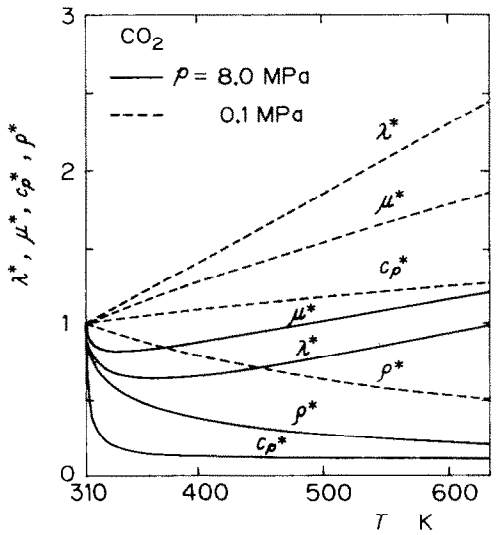

FIG. 5. Temperature- and pressure-dependence of thermophysical properties normalized with properties at 310 K.

Figure 7 shows the effect of the radial distance R and the temperature ratio T_w/T_j on the axial distribution of the radial velocity V and the temperature θ at $p_j = 0.1$ MPa and 8.4 MPa for $L = 2$, $Re = 1000$ and $T_j = 310$ K. In the figure, it is considered that $R = 0.25$ regards as the typical impinging-jet region, $R = 0.71$ as the transition region and $R = 4.0$ as the wall-jet region, and $L - X = 0$ means the impingement wall. The difference of the velocity V distribution between $p_j = 0.1$ MPa and 8.4 MPa is little more pronounced than that of the temperature θ distribution. As the temperature ratio T_w/T_j is increased, the velocity gradient and the temperature gradient of $p_j = 8.4$ MPa become steeper than those of $p_j = 0.1$ MPa.

Figure 8 shows the effect of the jet pressure on the local heat transfer coefficient at the stagnation point. As the temperature ratio T_w/T_j approaches unity, the heat transfer coefficient h_0 at the jet pressure $p_j = 0.1$ MPa decreases but the h_0 in the case of the supercritical jet pressures $p_j \geqslant 7.4$ MPa represents a sudden increase. Moreover, it can be seen from the figure that the stagnation-point heat transfer coefficient is increased 1.5- or 9-fold by increasing the jet pressure p_j from the atmospheric pressure of 0.1 MPa to a supercritical pressure of 8.4 MPa. The physical properties in the vicinity of the pseudocritical temperature T_{pc} at the supercritical state appear a remarkable peculiarity by little temperature change as shown in Figs. 4 and 5. In comparison with the pseudocritical temperature T_{pc} of each jet pressure p_j at the jet temperature $T_j = 310$ K in Fig. 8, the T_{pc} of $p_j = 8.4$ MPa becomes closer than that of $p_j = 7.4$ MPa. Therefore, it is considered that the stagnation-point heat transfer coefficient at $p_j = 8.4$ MPa is affected significantly by the temperature dependence of the physical properties. This enhancement of heat transfer in the supercritical state is due to the change of temperature field and the velocity field. Namely, as the fluid temperature approaches the pseudocritical temperature, noticeable changes of the specific heat and the thermal conductivity shown in Fig. 4 and the steep temperature gradient in the vicinity of the heat-transfer surface in Fig. 7 have direct effects upon the heat transfer. In case the T_j is close to the T_{pc} and as the temperature ratio T_w/T_j approaches unity, a ratio containing the region of pseudocritical temperature in the boundary layer increases; consequently, the enhancement of heat transfer appears remarkable. This tendency is pointed out in an experimental study of free convective heat transfer in supercritical carbon dioxide [18].

Figure 9 shows the effect of the jet temperature T_j on the heat transfer coefficient h_0 at the jet pressure $p_j = 8.0$ MPa. As the jet temperature approaches the

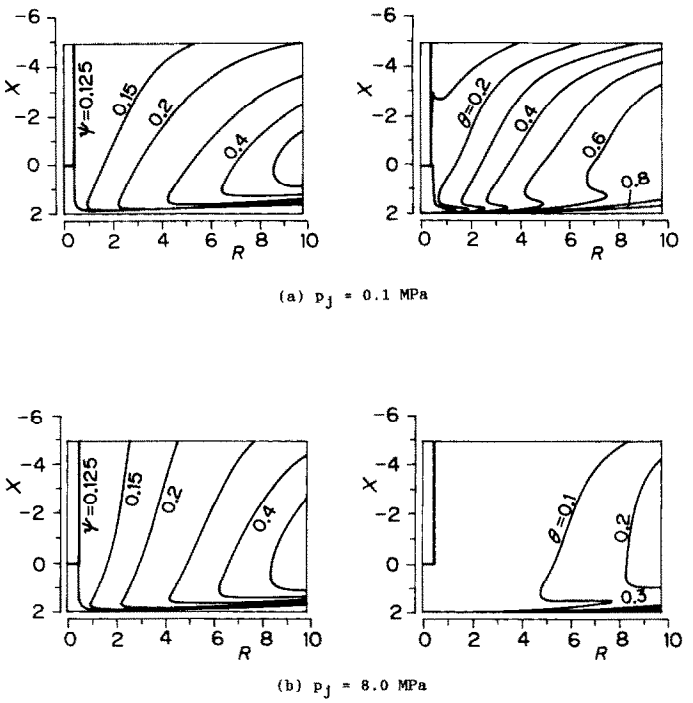

FIG. 6. Streamlines and isotherms for $L = 2$, $Re = 1000$, $T_j = 310$ K and $T_w = 315$ K. (a) $p_j = 0.1$ MPa; (b) $p_j = 8.0$ MPa.

pseudocritical temperature T_{pc} and the temperature ratio T_w/T_j to unity, the rapid increase of the h_0 is apparent. Therefore, it is practically advantageous to select the jet pressure so that the jet temperature may approach the pseudocritical temperature as closely as possible.

The stagnation-point heat transfer coefficient h_0 is quite insensitive to the jet-to-surface distance L, as shown in Fig. 10. The effect of the distance L becomes larger as the temperature ratio T_w/T_j is close to unity. However, the maximum variation in the stagnation-point heat transfer coefficient is not more than 10% at most between $L = 1$ and 4, regardless of the jet pressure, the jet temperature, and the jet Reynolds number. Accordingly, the present numerical calculations were performed mainly for the distance of $L = 2$.

The effects of the surface temperature T_w and the jet Reynolds number Re on the radial distribution of the local heat transfer coefficient h_x are shown in Figs. 11 and 12, respectively. As the radial distance from the stagnation point is increased, the h_x at the supercritical pressure decreases monotonically like the previous study for the atmospheric jet pressure [9]. In Fig. 11, the local heat transfer coefficient h_x increases as the surface temperature T_w approaches the pseudocritical temperature T_{pc} corresponding to the jet pressure, owing to the increase of portion which has the strong temperature-dependence of the physical properties in the boundary layer. Figure 12 shows the effect of the jet Reynolds number Re on the local heat transfer coefficient h_x. As the Re is increased, the h_x increases by the intensive exchange of momentum with the surrounding fluid over the impingement wall.

3.4. *General representation of local Nusselt numbers*

A fluid has its own peculiar temperature-dependent physical properties and it is a troublesome task to investigate the effects of physical properties for the fluid. Hence, it is helpful for practical application to find a method of predicting the heat transfer coefficient by a fluid with pressure- and temperature-dependence of physical properties from the constant property solution (CPS).

Figure 13 shows a typical comparison of the stagnation-point Nusselt number Nu_0 between the CPS and the variable property solution (VPS) based on the reference temperature of T_w and T_j at the supercritical pressure and the atmospheric pressure. In the figure, the $(Nu_0)_r$ of the VPS by choosing the reference temperature of physical properties which are included in the Reynolds number and the Nusselt number overestimates or underestimates to that of the CPS. Accordingly, the reference temperature method cannot be applied to the general representation of local Nusselt numbers due to an axisymmetric laminar impinging jet of supercritical carbon dioxide.

As the result of evaluating the various kinds of property ratio method for the specific heat, the thermal conductivity, the density and the viscosity of carbon dioxide, a correlating equation as expressed by equation (13) enables us to predict the local Nusselt number of the variable property solution from that of the CPS.

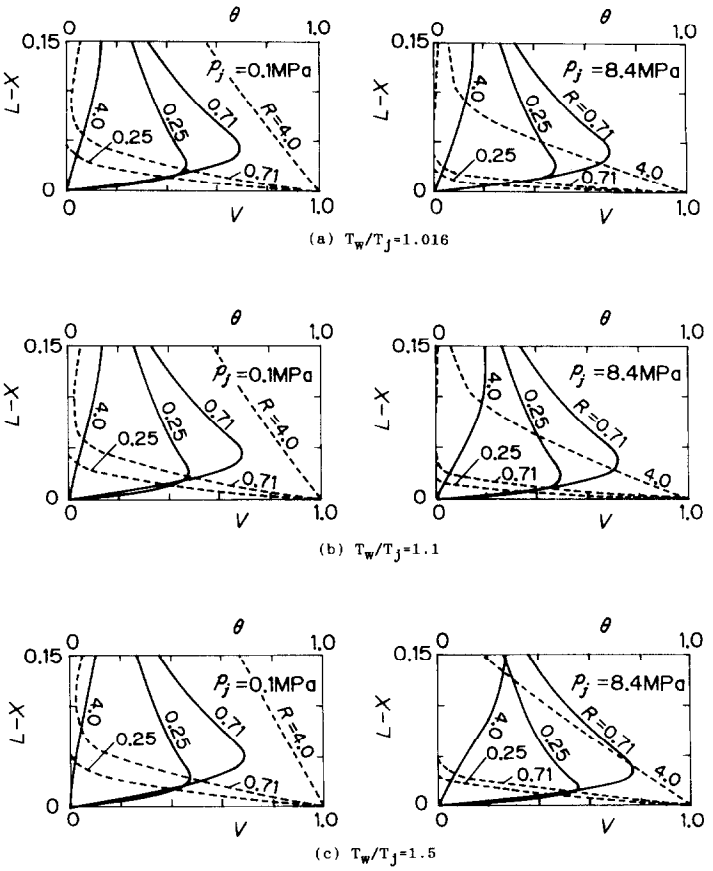

FIG. 7. Axial distribution of radial velocity V and temperature on impingement surface for $L = 2$, $Re = 1000$ and $T_j = 310$ K. In the legend, —— refer to V and – – – – to θ. (a) $T_w/T_j = 1.016$; (b) $T_w/T_j = 1.1$; (c) $T_w/T_j = 1.5$.

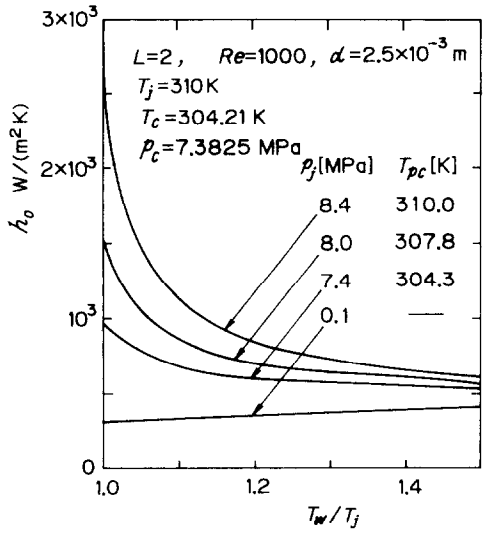

FIG. 8. Effect of the jet pressure p_j on the stagnation-point heat transfer coefficient.

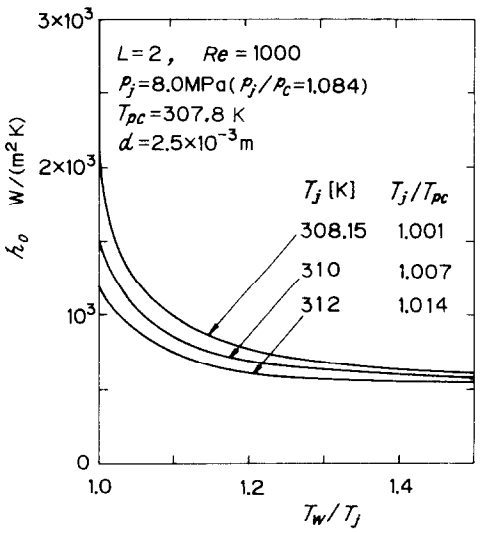

FIG. 9. Effect of the jet temperature T_j on the stagnation-point heat transfer coefficient.

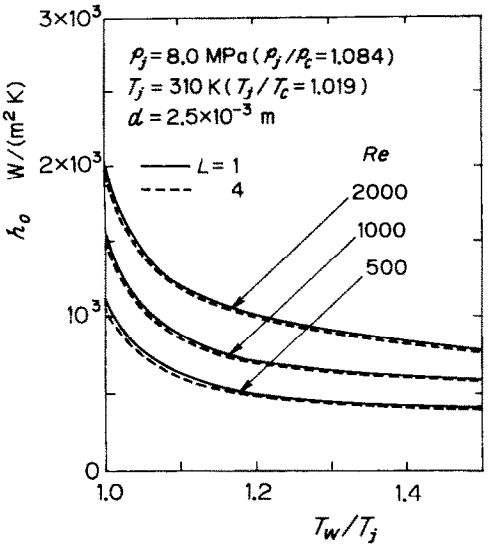

FIG. 10. Effect of jet-to-surface distance L on the stagnation-point heat transfer coefficient.

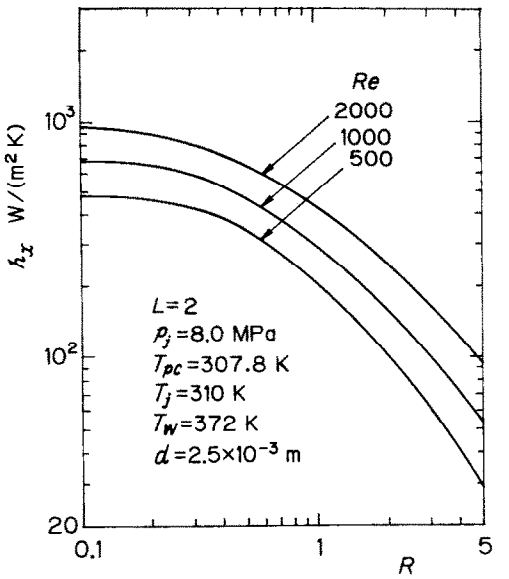

FIG. 12. Effect of the jet Reynolds number Re on the local heat transfer coefficient.

$$(Nu)_j^* = Nu\left(\frac{T_j}{T_{pc}}\right)^{7.2}\left(\frac{\rho_w}{\rho_j}\right)^{0.62}\left(\frac{Pr_w}{Pr_j}\right)^{0.15} \quad (13)$$

where Nu is the local Nusselt number obtained by the constant property solution and the stagnation-point Nusselt number Nu_0 can be obtained from the correlating equation (11). In Fig. 14, the stagnation-point Nusselt numbers of the VPS $(Nu_0)_j$ are compared with the approximate value $(Nu_0)_j^*$ obtained from equation (13). Equation (13) is applicable for the range of $1 \leqslant L \leqslant 4$, $500 \leqslant Re \leqslant 2000$, $1.005 \leqslant T_j/T_{pc} \leqslant 1.14$, and $1.02 \leqslant T_w/T_{pc} \leqslant 1.6$ within an error of 10%.

Figure 15 shows a typical comparison of the local Nusselt number Nu obtained by the CPS with the local Nusselt numbers Nu_r which are evaluated on the basis of two reference temperatures, respectively and of the correlating equation (13). The CPS result Nu can be obtained from the correlating equation in the authors' previous paper [9]. The radial distribution of the local Nusselt number evaluated by the correlating equation (13) agrees well with the CPS result.

4. CONCLUSIONS

A numerical analysis has been carried out on heat transfer due to an axisymmetric laminar impinging jet

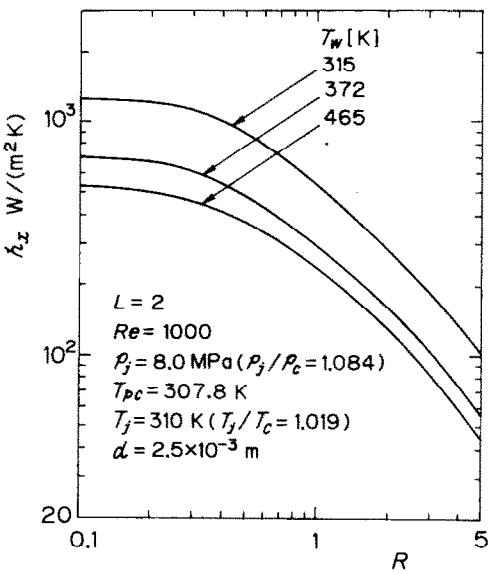

FIG. 11. Effect of the surface temperature T_w on the local heat transfer coefficient.

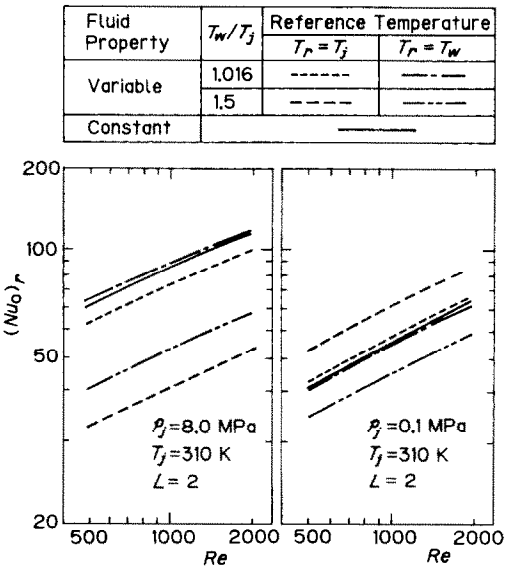

FIG. 13. Comparison in the stagnation-point Nusselt number between constant property solutions (CPS) and variable property solutions (VPS) based on the reference temperature of T_j and T_w.

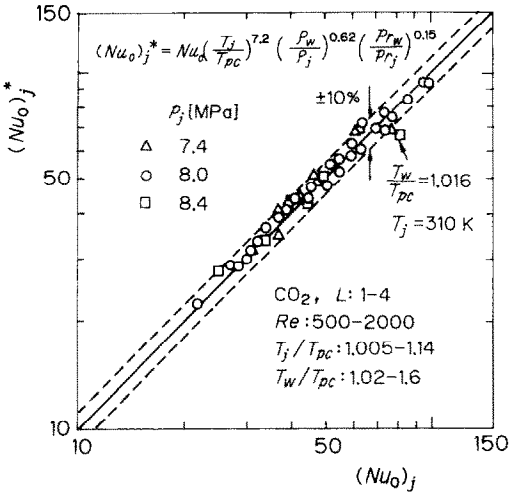

FIG. 14. Comparison in the stagnation-point Nusselt number between present solutions and results of correlating equation (13) for various supercritical jet pressures.

onto a flat surface of a uniform temperature, taking into account the pressure- and temperature-dependence of all physical properties of supercritical carbon dioxide. The present constant-property solutions for the local Nusselt number show good agreement with the existing experimental and theoretical results. The difference between the supercritical pressure and the atmospheric pressure for the flow field and temperature field are clarified. The stagnation-point heat transfer coefficient is increased 1.5- or 9-fold by increasing the jet pressure from the atmospheric pressure of 0.1 MPa to a supercritical pressure of 8.4 MPa in accordance with the difference of the pressure- and temperature-dependence of the physical properties. The jet-to-surface distance L has little influence on the stagnation-point Nusselt number for the supercritical jet pressure. It is practically advantageous to select the jet pressure so that the corresponding jet temperature may approach the pseudocritical temperature of the fluid as closely as possible. Also, a correlating equation by the property ratio method is proposed for generally predicting the local Nusselt number of the variable property solution from that of the constant property solution.

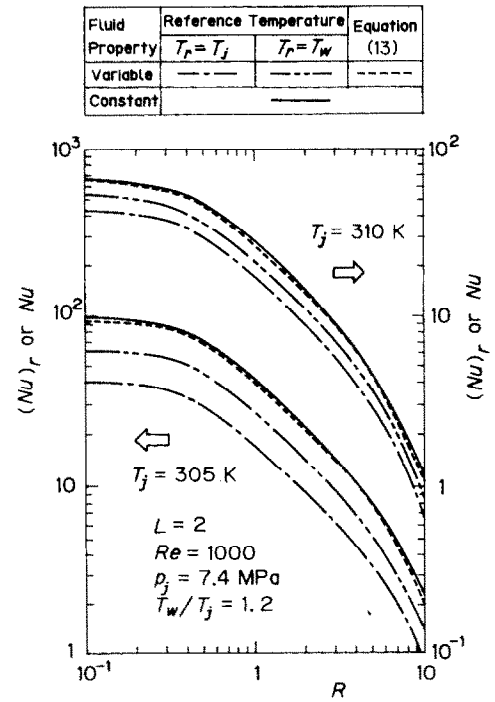

FIG. 15. Comparison in the local Nusselt number between the CPS and the VPS based on reference temperature methods and the property ratio method.

Acknowledgements—The authors wish to express their thanks to Professor T. Ito of Kyushu University for providing a copy of the PROPATH program package.

REFERENCES

1. H. Martin, Heat and mass transfer between impinging gas jets and solid surface. In *Advances in Heat Transfer* (Edited by J. P. Hartnett and T. F. Irvine), Vol. 13, pp. 1–60. Academic Press, New York (1977).
2. S. Yokobori, S. Kasaki and M. Hirata, Characteristic behaviour of turbulence in stagnation region on a two dimensional submerged jet impinging normally on a flat plate. In *Proc. Symp. in Turbulent Shear Flows* (Edited by M. Hirata *et al.*), pp. 3–17. Tokyo (1977).
3. K. Kataoka, T. Harada and R. Sahara, Mechanism for enhancement of heat transfer in turbulent impinging jets. In *Current Research in Heat and Mass Transfer* (Edited by M. V. K. Murthy *et al.*), pp. 81–96. Hemisphere, New York (1988).
4. M. T. Scholtz and O. Trass, Mass transfer in a non uniform impinging jet, Parts 1 and 2, *A.I.Ch.E. Jl* **16**, 82–96 (1970).
5. M. D. Deshpande and R. N. Vaishnav, Submerged laminar jet impingement on a plane, *J. Fluid Mech.* **114**, 213–236 (1982).
6. R. Echigo, H. Yoshida and T. Mochizuki, Temperature equalization by radiative converter for a slab in continuous casting-direct rolling, *Proc. 2nd ASME/JSME Thermal Engng Joint Conf.*, Vol. 5, pp. 22–27 (1987).
7. T. D. Yuan, J. A. Liburdy and T. Wang, Buoyancy effects on laminar impinging jets, *Int. J. Heat Mass Transfer* **31**, 2137–2145 (1988).
8. X. S. Wang, Z. Dagan and L. M. Jiji, Prediction of surface temperature and heat flux of a microelectronic chip with jet impingement cooling, *ASME Trans., J. Electronic Packaging* **112**, 57–62 (1990).
9. T. Aihara, J.-K. Kim and S. Maruyama, Effects of temperature-dependent fluid properties on heat transfer due to an axisymmetric impinging gas jet normal to a flat surface, *Wärme- und Stoffübertr.* **25**, 145–153 (1990).
10. W. B. Hall, Heat transfer near the critical point. In *Advances in Heat Transfer* (Edited by J. P. Hartnett and T. F. Irvine, Jr), Vol. 7, pp. 3–83. Academic Press, New York (1971).
11. S. Kakaç, The effect of temperature-dependent fluid properties in convective heat transfer. In *Handbook of Single-Phase Convective Heat Transfer* (Edited by S. Kakaç *et al.*), pp. 1–56. Wiley, New York (1987).
12. Japan Society of Mechanical Engineers, *JSME Data Book: Heat Transfer*, 4th Edn, pp. 89–90 (in Japanese). Maruzen, Tokyo (1986).
13. T. Aihara and J.-K. Kim, Heat transfer due to an axisym-

metric impinging jet of carbon dioxide in the near-critical region, *JSME Int. J. Ser. II* **34-2**, 175–182 (1991).
14. T. Ito and Propath Group, *PROPATH. A Program Package for Thermophysical Property*, ver. 3.1, Computer Center, Kyushu University, Fukuoka (1986).
15. S. V. Patankar, *Numerical Heat Transfer and Fluid Flow*. McGraw-Hill, New York (1980).
16. W. M. Pun and D. B. Spalding, A general computer program for two-dimensional elliptic flows, Report No. HTS/76/2, Dept. of Mech. Engng, Imperial College, London (1977).
17. W. M. Kays and M. E. Crawford, *Convective Heat and Mass Transfer*, 2nd Edn, pp. 275–287. McGraw-Hill, New York (1980).
18. R. J. Neumann and E. W. P. Hahne, Free convective heat transfer to supercritical carbon dioxide, *Int. J. Heat Mass Transfer* **23**, 1643–1652 (1980).

APPENDIX: EXAMINATION ON THE LOCATION OF BOUNDARIES BC AND CD

In this paper, the numerical calculations are performed for $L = 1$–4, $Re = 500$–2000, $p_j = 0.1$–8.4 MPa, $T_j = 305$–320 K and $T_w/T_j = 1.0$–1.5. The extremely remarkable conditions which the locations of the boundaries BC and CD in the present analysis have influence on the heat transfer characteristic and the velocity gradient over the impingement wall are as follows.

(1) The jet pressure p_j and temperature T_j are close to the critical point and moreover, the temperature ratio T_w/T_j is 1.1; in such a case, the effect of the temperature- and pressure-dependence of physical properties on the supercritical carbon dioxide appears markedly as shown in Figs. 4 and 5.

(2) The jet mouth-to-surface distance L is small and the jet Reynolds number Re is large; in such a case, the degree of the entrainment flow near the jet mouth contributes markedly to the flow in the vicinity of the wall.

Namely, the numerical solution in the case of $L = 1$, $Re = 2000$, $p_j = 7.4$ MPa, $T_j = 305$ K and $T_w/T_j = 1.1$ in the present study is represented by a strongly sensitive effect on the location of the calculation domain. In this condition, the effect on the local heat transfer coefficient h and the velocity gradient $(\partial V/\partial X)_w$ caused by the locations of boundaries BC and CD are shown in Figs. A1 and A2, respectively.

Figures A1(a) and A2(a) show the effect of the distance AB from the jet mouth to the boundary plane BC. In comparison to the result obtained by the AB $\to \infty$ extrapolation with the result by AB/$d = 6$ which is used in the present study, it

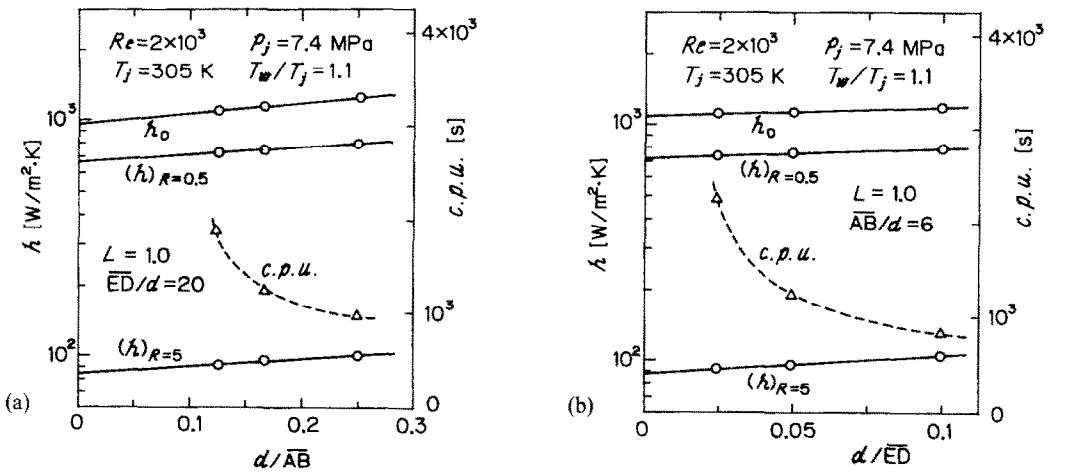

FIG. A1. Effect of the boundary location on the local heat transfer coefficient. (a) Boundary BC; (b) boundary CD.

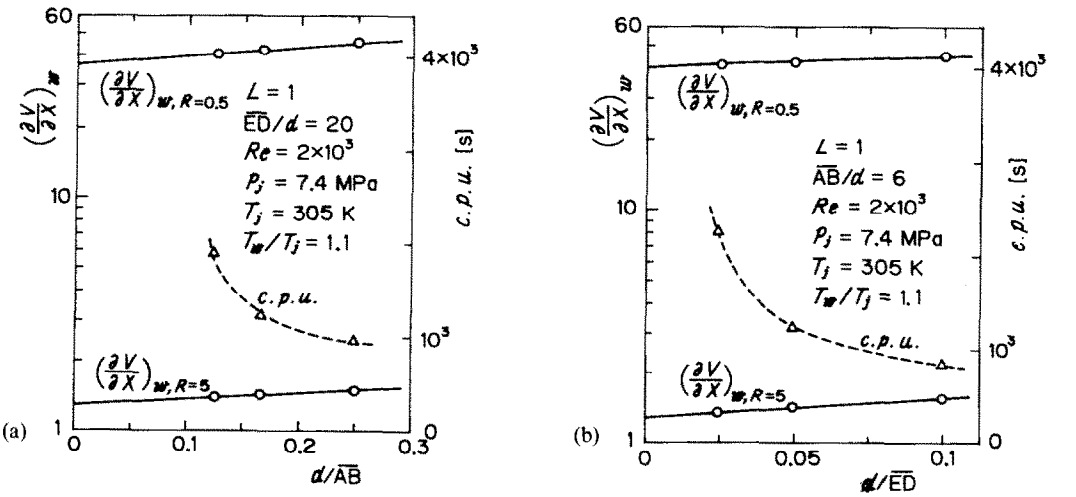

FIG. A2. Effect of the boundary location on the V-velocity gradient. (a) Boundary BC; (b) boundary CD.

seems to be probable that the local heat transfer coefficient at the stagnation point h_0 is overestimated under 17% and the value at $R = 5$, $(h)_{R=5}$ under 13%; the V-velocity gradient at $R = 0.5$, $(\partial V/\partial X)_{w,R=0.5}$ is over-estimated under 15% and the $(\partial V/\partial X)_{w,R=5}$ under 10%. Figures A1(b) and A2(b) represent the effect of the distance ED from the stagnation-point to the boundary plane CD. In comparison to the result obtained by the ED $\rightarrow \infty$ extrapolation with the result by ED/d = 20 which is used in the present study, it seems to be probable that the h_0 is overestimated under 3% and $(h)_{R=5}$ under 10%; the $(\partial V/\partial X)_{w,R=0.5}$ is overestimated under 6% and the $(\partial V/\partial X)_{w,R=5}$ under 10%.

As the boundaries BC and CD are located at the infinite distance, an accuracy of the numerical solution is increased; however, a rapid increase of the CPU time by the computation is also represented in Figs. A1 and A2. Therefore, since the relation of the accuracy and the computation expenses on the basis of the above-mentioned examination, the boundaries BC and CD of the solution domain in the present study are fixed at AB = 6d and ED = 20d.

ETUDE NUMERIQUE DU TRANSFERT THERMIQUE POUR UN JET LAMINAIRE AXISYMETRIQUE IMPACTANT DE DIOXYDE DE CARBONE SUPERCRITIQUE

Résumé—Les propriétés physiques d'un fluide supercritique varie fortement au voisinage du point critique. Le transfert thermique dû à un jet axisymétrique laminaire impactant une surface plane à température uniforme est analysé numériquement en prenant en compte la dépendance de toutes les propriétés physiques du dioxyde de carbone supercritique vis-à-vis de la température et de la pression. Des solutions numériques sont obtenues pour des nombres de Reynolds de jet 500–2000, des pressions 7,4–8,4 MPa, des distances de tuyère à surface 1–4 fois le diamètre de la tuyère, et une différence de température entre jet et paroi de 10 à 150 K. On étudie les différences entre la pression supercritique et la pression atmosphérique pour le champ d'écoulement et le champ de température. On examine les effets sur le transfert thermique de la pression et de la température de jet, de la différence de température entre sortie du jet et surface-cible et du nombre de Reynolds du jet. Une formule d'estimation de la valeur du nombre de Nusselt local est proposée pour le dioxyde de carbone supercritique par rapport à la solution de propriétés constantes et l'accord entre la formule et les résultats numériques est dans la marge de 10%.

NUMERISCHE UNTERSUCHUNG DES WÄRMEÜBERGANGS AUFGRUND EINES ACHSENSYMMETRISCHEN LAMINAREN AUFTREFFENDEN STRAHLS AUS ÜBERKRITISCHEM KOHLENDIOXID

Zusammenfassung—Die physikalischen Eigenschaften eines überkritischen Fluides ändern sich deutlich, wenn sich Temperatur und Druck dem kritischen Punkt annähern. In der vorliegenden Arbeit wird der Wärmeübergang beim Auftreffen eines achsensymmetrischen laminaren Strahls auf eine ebene Wandoberfläche von konstanter Temperatur numerisch untersucht, wobei die Temperatur- und Druckabhängigkeit aller physikalischer Eigenschaften des überkritischen Kohlendioxids berücksichtigt werden. Es werden numerische Lösungen für folgende Parameter ermittelt: Reynolds-Zahl des Strahls von 500–2000; Druck im Strahl von 7,4–8,4 MPa; Verhältnis zwischen dem Abstand der Düse von der Wand und dem Düsendurchmesser zwischen 1 und 4; Temperaturunterschied zwischen dem austretenden Strahl und der ebenen Wand zwischen 10 und 150 K. Der Einfluß der Differenz zwischen dem überkritischen Druck und Atmosphärendruck auf das Strömungsfeld und das Temperaturfeld wird untersucht. Ferner sind die Einflüsse des Strahldruckes, der Strahltemperatur, des Temperaturunterschiedes zwischen dem austretenden Strahl und der Oberfläche sowie der Reynolds-Zahl des Strahles auf den Wärmeübergang von Interesse. Es wird eine Korrelationsgleichung zur Bestimmung der örtlichen Nusselt-Zahl für überkritisches Kohlendioxid aus der Lösung mit konstanten Stoffeigenschaften vorgeschlagen. Die Übereinstimmung zwischen den so berechneten und den numerischen Werten liegt innerhalb 10%.

ЧИСЛЕННОЕ ИССЛЕДОВАНИЕ ТЕПЛОПЕРЕНОСА ОТ НАБЕГАЮЩЕА ОСЕСИММЕТРИЧНОЙ ЛАМИНАРНОЙ СТРУИ СВЕРХКРИТИЧЕСКОЙ ДВУОКИСИ УГЛЕРОДА

Аннотация—Физические свойства сверхкритической жидкости существенно изменяются по мере приближения температуры и давления к критической точке. В данной работе, принимая во внимание зависимость всех физических свойств сверхкритической двуокиси углерода от температуры и давления, численно исследуется теплоперенос при набегании осесимметричной ламинарной струи на плоскую стенку с однородной температурой. Получены численные решения для числа Рейнольдса в диапазоне 500–2000, давления струи—7,4–8,4 МПа, расстояния между началом струи и поверхностью—1–4 диаметра сопла, а также разности температур между началом струи и плоской стенкой, изменяющейся от 10 до 150 К. Исследуются различия между сверхкритическим и атмосферным давлениями для полей течения и температур. Кроме того, рассматривается влияние давления и температцры струи, разности температцр начала струи и поверхности, а также числа Рейнольдса струи на величину теплового потока. Предложено обобщающее соотношение для оценки значения локального числа Нуссельта для сверхкритической двуокиси углерода в растворе с постоянными свойствами, и получено согласие с численными результатами в пределах 10%.